EPJ manuscript No.
(will be inserted by the editor)

Calculations of ^{6}He+p elastic scattering cross sections using folding approach and high-energy approximation for the optical potential

K.V. Lukyanov[1], V.K. Lukyanov[1], E.V. Zemlyanaya[1], A.N. Antonov[2], and M.K. Gaidarov[2,3] [a]

[1] Joint Institute for Nuclear Research, Dubna 141980, Russia
[2] Institute for Nuclear Research and Nuclear Energy, Bulgarian Academy of Sciences, Sofia 1784, Bulgaria
[3] Instituto de Estructura de la Materia, CSIC, Serrano 123, E-28006 Madrid, Spain

Received: date / Revised version: date

Abstract. Calculations of microscopic optical potentials (OP's) (their real and imaginary parts) are performed to analyze the ^{6}He+p elastic scattering data at a few tens of MeV/nucleon (MeV/N). The OP's and the cross sections are calculated using three model densities of ^{6}He. Effects of the regularization of the NN forces and their dependence on nuclear density are investigated. Also, the role of the spin-orbit terms and of the non-linearity in the calculations of the OP's, as well as effects of their renormalization are studied. The sensitivity of the cross sections to the nuclear densities was tested and one of them that gives a better agreement with the data was chosen.

PACS. 24.10.Ht Optical and diffraction models – 25.60.-t Reactions induced by unstable nuclei – 21.30.-x Nuclear forces – 21.10.Gv Mass and neutron distributions

1 Introduction

The basic characteristics of the exotic nuclei, such as their charge and matter distributions have been tested, in particular, by studying differential and total reaction cross sections of the proton scattering on exotic nuclei in inverse kinematics. Nowadays, a substantial amount of experimental data exists for the cross sections of ^{6}He+p elastic scattering at different energies. For example, proton elastic scattering angular distributions were measured at incident energies less than 100 MeV/N for ^{6}He, namely 25.2 [1,2,3,4], 38.3 [5], 41.6 [6,7,8], and 71 MeV/N [9,10] and at energy of 700 MeV/N for He and Li isotopes (*e.g.* refs. [11,12,13,14,15]). The analyses of differential and total reaction cross sections have been performed using different phenomenological and microscopic methods and models of nuclear structure (see, *e.g.* refs. [9,10,11,12,13,14,15,16, 17,18,19,20,21]). We note also the microscopic analysis (refs. [22,23,24,25,26,27]) based on the "coordinate-space g-matrix folding method" [28] (and some modifications [29]), where non-local OP is obtained using a folding of a local medium-dependent NN effective interaction with the target ground-state mixed density. In some of the calculations (*e.g.* [9,10,16,17]) the eikonal approach using proton and neutron density distributions, as well as parametrized NN total cross section have been used. It has been accepted that for energies larger than 500 MeV/N the multiple scattering diffraction theory developed in [30,31] (the Glauber theory) is a relevant method to study charge and matter distributions from proton elastic scattering data [11,32,33].

The experimental information on cross sections of ^{6}He+p elastic scattering requires for its adequate description a development of the respective microscopic methods of their analysis. These methods give an opportunity, first, to distinguish between different models for the exotic ^{6}He as a nucleus with a halo with two neutrons and, secondly, to test the attempts of the folding approach for constructions of optical potentials. The latter include the understanding of the role of various components of the OP and the necessity to introduce fitting parameters. A number of works has been devoted to calculations of OP's using the folding approach (see, *e.g.* [20,21,22,23],[34,35, 36,37,38]). For instance, the real parts of OP's for calculating the ^{6}He+p, ^{6}He+ ^{4}He (E_{lab}=151 MeV) [20] and ^{6}He+p, ^{8}He+p ($E_{inc} < 100$ MeV) [21] elastic differential cross sections have been obtained microscopically using realistic M3Y-Paris effective NN interaction [35,38,39] together with the Tanihata *et al.* proton and neutron densities of the helium isotopes [40] in refs. [20,21] and also with the densities of the cluster-orbital shell-model approximation (COSMA) [9,10,18,19]. In [21] a comparison of the obtained results has been performed to those from the alpha-core approach with the complex and fully non-local effective interaction [22] and also with the non-core model

[a] *e-mail: gaidarov@inrne.bas.bg* Present address: Insert the address here if needed

based on the large-scale shell-model (LSSM) calculations (refs. [7,36,37] and references therein). It was shown that the elastic scattering is a good tool to distinguish between different density distributions [21]. Usually, in the usage of the complex OP's for analyses of the differential cross sections, their imaginary part and the spin-orbit terms have been determined in a phenomenological way, and then the OP's include a number of fitting parameters. The question to optimize this number in the analyses of the experimental data is not usually considered.

The main aim of the present work is to calculate differential cross sections of elastic ^{6}He+p scattering at different energies studying the possibility to describe the existing experimental data by using a minimal number of fitting parameters. We note that for this purpose we use the so-called high-energy approximation (HEA) OP [41]. Its form can be considered as a microscopic folding of the densities of the colliding nuclei NN scattering amplitude. There are no free fitting parameters in this OP and its dependence on the energy is included in the input data of the NN scattering amplitude and the total cross section. It is generally believed that the Glauber (eikonal) approximation is reasonable at energies of hundreds MeV and higher. However, beginning from the work [42] the method of HEA has been usually modified by replacing the eikonal straight-line trajectory at an impact parameter b by the parameter b_c that corresponds to the distance of the closest approach of the projectile in the Coulomb plus the nuclear potential. For the medium and heavy nuclei the Coulomb distortion dominates and successful applications of the approach were demonstrated, firstly, in [43] and later on in many papers, *e.g.* in [41,44,45,46] at low ($>$ 10 MeV/N) and intermediate energies to the description of the data on the differential elastic and total reaction cross sections of various projectile ions and target nuclei. The distortion effect caused by the nuclear potential is important mainly for lightest nuclei as shown in [47]. In the last decade such a modified Glauber method turned out to be rather effective and was employed in many works devoted to analyses of nucleus-nucleus scattering processes. In the present paper, to avoid limitations in the modified HEA formulae, we account for distortion effects by computing cross sections using the DWUCK4 code of numerical solving of the Schrödinger equation. At the same time we use (similarly to ref. [48]) the microscopic HEA imaginary part of the OP obtained in ref. [41] that yields the same eikonal phase as that given in the optical limit of the Glauber microscopic theory of multiple scattering of complex systems. So, one of the main aims of our work is to establish the limits of the applicability of the HEA OP for calculations of differential elastic cross sections of the ^{6}He+p scattering for different regions of angles and incident energies. Together with the HEA imaginary potential we tested the OP whose form coincides with that of the real part of the standard folding OP [34,35,38]. The latter includes an exchange term and, correspondingly, the non-linear effects in calculations of the potential. In the calculations we pay attention to the role of the importance of the contribution of various physical quantities and features, such as microscopically obtained spin-orbit forces and regularization of the NN forces used in folding calculations. Also, we consider effects of renormalization of the real and imaginary parts of microscopic optical potentials, the differences or similarities of various models for the ^{6}He structure which are used in the description of the experimental data on the cross section of the ^{6}He+p elastic scattering.

The theoretical scheme for microscopical calculations of the real part of the OP's and cross sections is given in sect. 2. This sect. includes also some methodical calculations. Section 3 is devoted to the OP within the HEA. The results of the calculations and the discussion are presented in sect. 4. Section 5 includes the conclusions from the work.

2 Basic relationships for calculations of the real part of the nucleon-nucleus optical potential

2.1 Direct part of the real OP (Re OP)

The real part of the nucleon-nucleus OP is assumed to be a result of a single folding of the effective NN potential with the nuclear density, *i.e.* this is a particular case of the double-folding [34] in which a $\delta(\mathbf{r}_1)$ function has to be used for the density of the incoming particle $\rho(\mathbf{r}_1)$. Then the direct part of the Re OP (V^D) has the following form of the isoscalar (IS)- and isovector (IV)- contributions, correspondingly:

$$V^D_{IS}(r) = \int \rho_2(\mathbf{r}_2) g(E) F(\rho_2) v^D_{00}(s) d^3 r_2, \qquad (1)$$

$$V^D_{IV}(r) = \int \delta\rho_2(\mathbf{r}_2) g(E) F(\rho_2) v^D_{01}(s) d^3 r_2, \qquad (2)$$

where $\mathbf{s} = \mathbf{r} + \mathbf{r}_2$,

$$\rho_2(\mathbf{r}_2) = \rho_{2,p}(\mathbf{r}_{2,p}) + \rho_{2,n}(\mathbf{r}_{2,n}), \qquad (3)$$

$$\delta\rho_2(\mathbf{r}_2) = \rho_{2,p}(\mathbf{r}_{2,p}) - \rho_{2,n}(\mathbf{r}_{2,n}). \qquad (4)$$

Here $\rho_{2,p}(\mathbf{r}_{2,p})$ and $\rho_{2,n}(\mathbf{r}_{2,n})$ are the proton and neutron densities in the target nucleus. In eqs. (1) and (2) $g(E) = 1 - 0.003E$ represents the energy dependence of the effective NN interaction while $F(\rho_2)$ contains its density dependence. Following ref. [38] we use its form for the CDM3Y6 effective Paris potential:

$$F(\rho) = C\left[1 + \alpha e^{-\beta\rho(\mathbf{r})} - \gamma\rho(\mathbf{r})\right], \qquad (5)$$

where $C = 0.2658$, $\alpha = 3.8033$, $\beta = 1.4099$ fm^3, $\gamma = 4.0$ fm^3.

The effective NN interaction $v^D_{00(01)}$ in eqs. (1) and (2) has included the isoscalar and isovector components of the direct part of the M3Y interaction based on the results of the g-matrix calculations using the Paris NN potential [35,38]. The M3Y potentials which are used in the folding calculations of OP's are sums of Yukawa-type terms

$\exp(-\mu r)/(\mu r)$. Using eqs. (1)-(5) one can obtain the following forms of the direct part of the isoscalar Re OP expressed by integrals in the coordinate and momentum space, correspondingly:

$$V_{IS}^{D}(r) = Cg(E)\int\Big[\rho_2(\mathbf{r}_2) + \alpha\bar{\varrho}_2(\mathbf{r}_2) - \gamma\tilde{\varrho}_2(\mathbf{r}_2)\Big] \times v_{00}^{D}(s)d^3r_2, \quad (6)$$

$$V_{IS}^{D}(r) = \frac{Cg(E)}{2\pi^2}\int_0^\infty\Big[\rho_2(q) + \alpha\bar{\varrho}_2(q) - \gamma\tilde{\varrho}_2(q)\Big] \times v_{00}^{D}(q)j_0(qr)q^2dq, \quad (7)$$

where $\bar{\varrho}_2(\mathbf{r}_2), \tilde{\varrho}_2(\mathbf{r}_2)$ and their Fourier transform have the forms:

$$\bar{\varrho}_2(\mathbf{r}_2) = \rho_2(\mathbf{r}_2)e^{-\beta\rho_2(\mathbf{r}_2)}, \quad (8)$$

$$\tilde{\varrho}_2(\mathbf{r}_2) = \big[\rho_2(\mathbf{r}_2)\big]^2, \quad (9)$$

$$\rho(q) = \int e^{i\mathbf{qr}}\rho(r)d^3r = 4\pi\int_0^\infty \rho(r)j_0(qr)r^2dr. \quad (10)$$

Similarly, exchanging ρ_2 by $\delta\rho_2$ [eq. (4)] one can obtain the isovector part V_{IV}^{D} of the direct part Re OP.

2.2 Exchange part of the real OP (Re OP)

In contrast to the case of the double-folding potential where integration over the coordinates ($\mathbf{r}_1$) of the nucleons in the incoming nucleus takes place, in the case of the nucleon-nucleus interaction one can obtain:

$$V_{IS}^{EX}(r) = g(E)\int\rho_2(\mathbf{r}_2, \mathbf{r}_2 - \mathbf{s})F\left(\rho_2(\mathbf{r}_2 - \mathbf{s}/2)\right) \times v_{00}^{EX}(s)j_0(k(r)s)d^3r_2. \quad (11)$$

For the density matrix $\rho_2(\mathbf{r}_2, \mathbf{r}_2 - \mathbf{s})$ in eq. (11) we use the approximation for the calculation of the knock-on exchange term of the folded potential from [49] which preserves the first term of the expansion given in [50]:

$$\rho_2\big(\mathbf{r}_2, \mathbf{r}_2 - \mathbf{s}\big) \simeq \rho_2\big(|\mathbf{r}_2 - \mathbf{s}/2|\big)\hat{j}_1\big(k_{F,2}(|\mathbf{r}_2 - \mathbf{s}/2|)\cdot s\big). \quad (12)$$

In eqs. (11) and (12):

$$\hat{j}_1(x) = \frac{3}{x}j_1(x) = \frac{3}{x^3}(\sin x - x\cos x), \quad (13)$$

$$F(\rho_2) = C\left[1 + \alpha e^{-\beta\rho_2(\mathbf{r}_2 - \mathbf{s}/2)} - \gamma\rho_2(\mathbf{r}_2 - \mathbf{s}/2)\right]. \quad (14)$$

In our case $\mathbf{r}+\mathbf{r}_2 = \mathbf{s}$, therefore $|\mathbf{r}_2 - \mathbf{s}/2| = |\mathbf{r} - \mathbf{s}/2| = |\mathbf{x}_2|$ and making the substitution $\mathrm{d}^3\mathbf{r}_2 = \mathrm{d}^3\mathbf{s}$ at fixed $\mathbf{r}$, eq. (11) can be rewritten in the form:

$$V_{IS}^{EX}(r) = g(E)\int h_2(\mathbf{r} - \mathbf{s}/2, \mathbf{s})F\left(\rho_2(|\mathbf{r} - \mathbf{s}/2|)\right) \times v_{00}^{EX}(s)j_0(k(r)s)d^3s, \quad (15)$$

where

$$h_2(\mathbf{x}_2, \mathbf{s}) = \rho_2(\mathbf{x}_2)\hat{j}_1\big(k_{F,2}(\mathbf{x}_2)\cdot s\big), \quad (16)$$

$\mathrm{d}^3s = s^2\mathrm{d}s\sin\theta\mathrm{d}\theta\mathrm{d}\phi$, with θ, ϕ being angles which determine the vector $\mathbf{s}/2$ with respect to the fixed vector $\mathbf{r}$. Integrating over $d\phi$ gives the factor 2π. We separate the integral over $\mathrm{d}x = \sin\theta\mathrm{d}\theta = -\mathrm{d}\cos\theta$:

$$G_0^{IS}(r,s) = \int_{-1}^{1}\rho_2\big(x_2(r,s,x)\big)\,\hat{j}_1\big(k_{F,2}\left(x_2(r,s,x)\right)\big) \times F\big(\rho_2\left(x_2(r,s,x)\right)\big)\,dx, \quad (17)$$

where

$$x_2(r,s,x) = |\mathbf{r} - \mathbf{s}/2| = \left[r^2 + \frac{s^2}{4} + rsx\right]^{1/2}. \quad (18)$$

Finally, the isoscalar part of the exchange Re OP of the nucleon-nucleus interaction has the form:

$$V_{IS}^{EX}(r) = 2\pi g(E) \times \int G_0^{IS}(r,s)v_{00}^{EX}(s)j_0\left(k(r)s\right)s^2ds. \quad (19)$$

In eqs. (11) and (19), $v_{00}^{EX}(s)$ is the isoscalar part of the exchange contribution to the effective NN interaction and the local momentum of the incident nucleon in the field of the Coulomb and nuclear potential (Re OP) is [51]:

$$k^2 = (2m/\hbar^2)\left[E_{c.m.} - Vc(r) - V(r)\right]\left[\frac{1 + A_2}{A_2}\right]. \quad (20)$$

In eqs. (12), (16) and (17) $k_{F,2}$ defines the average relative momentum [49,51]:

$$k_{F,2}(r) = \left\{\frac{5}{3\rho}\left[\tau(\rho) - \frac{1}{4}\nabla^2\rho(r)\right]\right\}^{1/2}, \quad (21)$$

where we choose further the extended Thomas-Fermi approximation [52,53] for the kinetic energy density

$$\frac{\tau(\rho)}{2} \simeq \tau_q(\rho_q) = \frac{3}{5}\left(3\pi^2\right)^{2/3}\left[\rho_q(r)\right]^{5/3} + \frac{|\nabla\rho_q(r)|^2}{36\rho_q(r)} + \frac{\nabla^2\rho_q(r)}{3}, \quad (22)$$

valid for each kind of particles $q = n, p$.

The isovector part of the exchange Re OP can be obtained from eqs. (17) and (19) exchanging ρ_2 by $\delta\rho_2$.

2.3 "Regularization" of the effective NN interaction in the form of Yukawa potential

An important aspect of using the M3Y effective NN potentials in their traditional form

$$v(s) = \sum_j N_j\frac{\exp(-\mu_j|s|)}{\mu_j|s|} \quad (23)$$

is related to their regularization due to the singularities. The latter aims to exclude the singularities at the point $|\mathbf{s}| = 0$, which have no physical meaning. Formally, this

singularity might affect the consideration of the nucleon-nucleon scattering, but it does not cause any difficulties in the calculations of the folding integral [*e.g.* eqs. (6) and (15)] to generate the nucleon-nucleus and/or nucleus-nucleus potential. Nevertheless, "regularized" M3Y potentials of the NN interaction which do not contain the mentioned singularity have been used in some works (*e.g.* [21, 54]) and in our work we would like to consider this point in more details. Note that the physical reason for that kind of problems is related to the breaking of the meson theory at very short range due to the extended structure of nucleons [55]. That is why the one-boson-exchange potentials are usually regularized by introducing, *e.g.*, the monopole-, dipole-, exponential cut-off form factors [56], as well as that suggested in ref. [57]. As shown in [58], the most important feature of these form factors is that they have the same principal range, and that the overall results are insensitive to their detailed shape. In refs. [21,54] cut-off form factor was taken to be equal to the proton form factor $\rho_p(q)$, parametrized according to the experimental data in [59] as a sum of Gaussian functions. As a test of the role of the regularization, in the present work we take the same expression, and then use the corresponding "smoothing" function in a coordinate space, which has a meaning of the density distribution of the incoming proton

$$\rho_p(r) = \sum_{i=1}^{3} a_i \frac{1}{(\pi r_i^2)^{3/2}} \exp\left(-\frac{r^2}{r_i^2}\right), \qquad (24)$$

where $\sum a_i = 1$, a_1=0.506373, a_2=0.327922, a_3=0.165705, $r_1^2 = 0.431566$ fm^2, $r_2^2 = 0.139140$ fm^2, $r_3^2 = 1.525540$ fm^2, and $\langle r^2\rangle$=0.77542 fm^2. Then, the regularized NN potential is determined by

$$v_{reg}(s_1) = \int \rho_p(r_1) v(s) d^3 r_1, \qquad \mathbf{s}_1 = \mathbf{r}_1 + \mathbf{s}. \qquad (25)$$

Rewriting this integral in the momentum representation one gets the expression used in [21,54] instead of $v(s)$

$$v_{reg}(s_1) = \frac{1}{(2\pi)^3} \int \rho_p(q)\, v(q)\, e^{i\mathbf{q}\mathbf{s}_1} d^3 q, \qquad (26)$$

where the proton form factor

$$\rho_p(q) = \int e^{-i\mathbf{q}\mathbf{r}_1} \rho_p(r_1) d^3 r_1 = \sum a_i \exp\left(-\frac{q^2 r_i^2}{4}\right) \qquad (27)$$

and

$$v(q) = \sum_j N_j \frac{4\pi}{\mu_j} \frac{1}{\mu_j^2 + q^2}. \qquad (28)$$

On the other hand, substituting the "regularized" $v_{reg}(s_1)$ potential (25) in eq. (1) instead of $v(s)$ leads to the expression

$$V_{IS}^D(r) = \int \rho_p(\mathbf{r}_1) g(E) F(\rho) v_{00}^D(s) \rho_2(\mathbf{r}_2) d^3 r_1 d^3 r_2, \quad \mathbf{r}_1 + \mathbf{s} = \mathbf{r} + \mathbf{r}_2, \qquad (29)$$

whose form coincides with the definition of the double-folding potential of interaction of two colliding complex systems having densities ρ_p and ρ_2.

2.4 Methodical calculations

In this subsection we will present results of our calculations of the ^{6}He+p elastic scattering differential cross sections studying the role of various factors, such as: i) the choice of the density distribution of ^{6}He, ii) effects of the regularization, and iii) the effect of the spin-orbit term in its dependence on the interaction potential.

In the calculations we use the following three density distributions of ^{6}He:

i) the point-nucleon density

$$\rho_{point}^X = \frac{2}{\pi^{3/2}} \left\{ \frac{1}{a^3} \exp\left[-\left(\frac{r}{a}\right)^2\right] + \frac{1}{b^3} \frac{X-2}{3} \left(\frac{r}{b}\right)^2 \exp\left[-\left(\frac{r}{b}\right)^2\right] \right\} \qquad (30)$$

applied by Tanihata *et al.* [60] for a comparison of the measured total reaction cross section of ^{6}He+^{12}C at 800 A MeV with the respective expression from [61] obtained there in the optical limit of the Glauber theory. In (30) $X = Z, N$, and the parameter values of a and b are determined from

$$a^2 = a^{*2}\left(1 - \frac{1}{A}\right), \qquad b^2 = b^{*2}\left(1 - \frac{1}{A}\right), \qquad (31)$$

where a^* = 1.53 fm, b^* = 2.24 fm, and hence a = 1.40 fm, b = 2.04 fm. Thus, the rms radius of the point-proton density of ^{6}He is equal to 1.72 fm.

ii) the COSMA point-nucleon density [19] which has the same analytical form as eq. (30), but with the parameter values a = 1.55 fm and b = 2.24 fm [9,10], and the rms radius of the point-proton density is equal to 1.89 fm.

We should emphasize that both Tanihata and COSMA densities have a Gaussian asymptotic behavior which is not a realistic one at high q. That is why we consider also other more realistic proton and neutron densities of ^{6}He:

iii) the LSSM densities obtained in a complete $4\hbar\omega$ shell-model space [36] using Woods-Saxon (WS) single-particle wave function basis with realistic exponential asymptotic behavior.

In fig. 1 we present the total density distribution of ^{6}He: $\rho(r) = \rho_p(r) + \rho_n(r)$ (in logarithmic and linear scale), as well as the point-proton and point-neutron density distributions of Tanihata *et al.*, COSMA and LSSM. One can see that the Tanihata and COSMA densities have a Gaussian slope while the LSSM tail occurs too higher and goes for the neutrons to larger values of r than for protons. As known, the differences between the densities for smaller values of r ($r < R$, R being the linear size of the nucleus) can be revealed mostly in the nucleon-nucleus scattering, but in heavy ion collisions one can study better the asymptotic region.

The role of the regularization (described in subsect. 2.3) is shown in fig. 2 by a comparison of the ^{6}He+p elastic scattering differential cross sections at different energies: 25.2, 41.6, and 71 MeV/N. As can be seen, generally the effect of the regularization is rather weak, but it increases when the energy and the scattering angle increase.

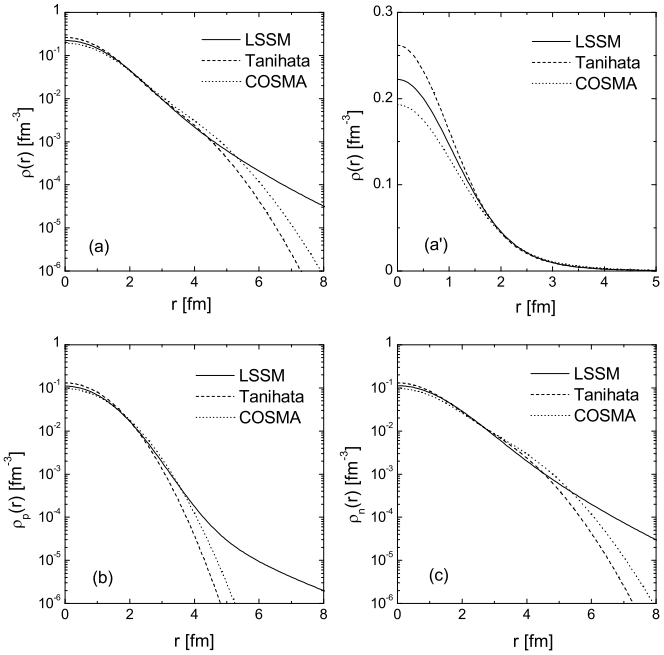

Fig. 1. Total ((a) and (a′)) , point-proton (b) and point-neutron (c) densities from the model of Tanihata *et al.* [60], COSMA [19] and LSSM calculations [36].

It starts to be seen at smaller angles when the energy increases. Generally, checking the role of the regularization we conclude that it is not necessary to include it in the cases of folding OP's in the nucleon-nucleus scattering.

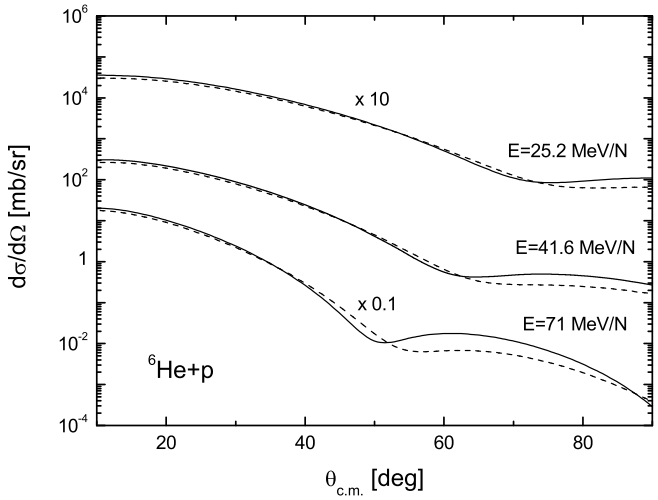

Fig. 2. Elastic ^{6}He+p scattering cross sections at different energies computed by using the microscopically folded real OP and the imaginary part taken in the same form ($V^F = V^D + V^{EX}$) calculated using the LSSM density of ^{6}He with (dashed line) and without (solid line) regularization of the M3Y effective NN interaction.

In fig. 3 we show the role of the spin-orbit term in the cross section of elastic ^{6}He+p scattering at a given energy $E = 41.6$ MeV/N. The spin-orbit term is taken to be in the form:

$$U_{so} \simeq N_{so}\lambda_\pi^2 \left(\frac{1}{r}\right)\frac{df(r)}{dr}, \qquad (32)$$

where $f(r)$ is the form of the Re OP, and λ_π^2=2 fm^2. The calculations are given for three cases: i) when $N_{so} = 0.5$ and $f(r)$ is exchanged by the microscopic Re OP=$V^{micro}(r)$ in MeV; ii) $N_{so} = 6.2$ MeV and $f(r)$ is the WS form factor taken from [62], and iii) without spin-orbit term, *i.e.* when $N_{so} = 0$.

One can see that the cross sections in the cases i) and ii) are very close to each other. Our analysis showed that, generally, there is not a strong dependence on the shape of $f(r)$. From the other side, however, the effect of the spin-orbit term in the considered case is important at larger angles ($> 60°$).

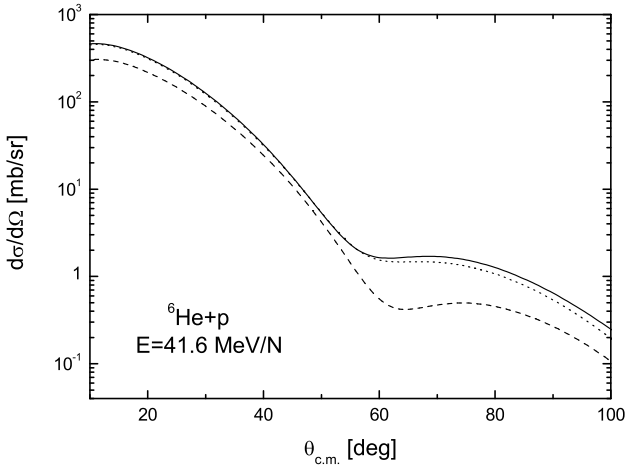

Fig. 3. Elastic ^{6}He+p scattering cross section at energy $E = 41.6$ MeV/N calculated using the microscopic Re OP (V^F) in the spin-orbit term $(1/r)\mathrm{d}V^F/\mathrm{d}r$ (solid line) and also using the WS Re OP in $12.4(1/r)\mathrm{d}f^{WS}/\mathrm{d}r$ (dotted line). The dashed line shows calculations without spin-orbit term. The LSSM density is taken for ^{6}He and the Im OP has the form of V^F.

3 Optical potential within the high-energy approximation

As known, the real part of the optical potential can be calculated microscopically in the standard form of the single- or double-folded integral. In principle, the physical nature of the real and imaginary parts of OP is different. The imaginary part is related to the flux loss at the transition of the particles from the elastic to the inelastic and reaction channels which depends on both the structure of the colliding nuclei and reaction mechanisms. This makes it difficult to construct practically a convenient theory of the Im OP especially for nucleus-nucleus scattering (see, *e.g.*,

[63] and refs. therein). However, in the case of more simple proton-nucleus scattering one can get fairly good applications (see, *e.g.*, [64]) when using a single-folding pseudopotential [34] multiplied by the fitted complex renormalization factor $(N_R + iN_I)$ to obtain the complex potential with the unit shape of the real and imaginary parts. On the other hand, in the case of heavy ion scattering, many applications were made when the real part of OP was microscopically calculated while an imaginary part was taken in the WS form with three or more fitted parameters.

In this paper we intend to test the so-called HEA optical potential (at least its imaginary part) to explain the available data on the ^{6}He+p differential cross sections at a few tens of MeV/N. As already mentioned in the Introduction, the generalization of the eikonal method made it possible to use it at relatively low energies [41,42,43,44, 45,46,47]. In our work, on the base of the eikonal phases we reconstruct the equivalent potential including its imaginary part. The calculations of the cross sections are performed *by numerical integration of the Schrödinger equation* by means of the code DWUCK4 using all interactions obtained (Coulomb plus nuclear OP), but not using the HEA scheme for cross section calculations. We note that using this method we aim to establish *the limits of the applicability of the imaginary part of the HEA optical potential*. We also note that, firstly, in the calculations of the HEA potential, similarly to ref. [41,48], we do not neglect the parallel contribution of the transferred momentum (in contrast to the Glauber method). As a result, the integral in the expression for the potential includes spherical Bessel functions, instead of the cylindrical ones (which appear in the expressions for the eikonal HEA). Secondly, this makes softer the limitation of the applicability of the method. We mention that in this case the region of the applicability of the standard HEA for $E \gg |U(\bar{R})|$ and small angles is transformed to $E < |U(\bar{R})|$ and $\vartheta < [\sqrt{2/k\bar{R}} + |U(\bar{R})|/E]$, with $\bar{R}$ being the radius of the potential at its periphery (*e.g.* at the half-depth of the nuclear potential), where the absorption is quite strong [65]. Previously, the microscopic HEA OP was successfully applied in refs. [41,66,67] to describe the ^{16,17}O+A elastic scattering data at about hundred of MeV/N from [68,46]. Here we would like to give an estimation for the angles of the application of our approach. For the ^{6}He+p scattering at E_{lab}=40 MeV/N and $\bar{R} \approx 2$ fm, it follows from the expression given above that $\vartheta < 50°$, *i.e.* this is the applicability region of angles considered in our calculations. The basic component of HEA is the eikonal phase $\Phi(b)$ which depends on the impact parameter of the collision b. The amplitude and the cross sections of scattering and reactions are expressed by means of $\Phi(b)$. In the phenomenological approach the phase is given by the integral along the axis z of the interaction potential. On the other side, this phase was derived in the microscopic level for the proton-nucleus scattering in the Glauber theory [30,31] and generalized later to the nucleus-nucleus scattering in [69,70]. In the so-called "optical limit" of this theory an explicit form of the microscopical phase $\Phi(b)$ is expressed by the densities of colliding nuclei and of the amplitude of the NN scattering. By a comparison of both the eikonal and microscopic expressions for the phase it became possible in [41] and [48] to obtain the explicit form of the OP in HEA, which gives a description of the nucleus-nucleus scattering, being equivalent to that from the microscopical approach:

$$U^H_{opt} = V^H + iW^H, \tag{33}$$

where

$$V^H(r) = -\frac{\hbar v}{(2\pi)^2}\bar{\sigma}_{NN}\bar{\alpha}_{NN} \times \int_0^\infty \rho_1(q)\rho_2(q)f_N(q)j_0(qr)q^2dq, \tag{34}$$

$$W^H(r) = -\frac{\hbar v}{(2\pi)^2}\bar{\sigma}_{NN} \times \int_0^\infty \rho_1(q)\rho_2(q)f_N(q)j_0(qr)q^2dq, \tag{35}$$

with v being the velocity of the nucleus-nucleus relative motion, $\rho_{1,(2)}(q)$ being the form factors corresponding to the point-like nucleon density distributions of the nuclei and $f_N(q)$ being the amplitude of the NN scattering which depends on the transfer momentum q (see, *e.g.* [71]). The quantities $\bar{\sigma}_{NN}$ and $\bar{\alpha}_{NN}$ are the averaged over the isospins total NN cross section and the ratio of the real to imaginary part of the scattering amplitude at zero angle of free nucleons. They can be obtained from the data on the mutual scattering of nucleons. For instance, the parametrizations of the energy dependence of $\bar{\sigma}_{NN}$ [44] and $\bar{\alpha}_{NN}$ in the interval $\epsilon_{lab} = 10$ MeV$\div$ 1 GeV [72] are known:

$$\bar{\sigma}_{NN} = \frac{Z_1Z_2\sigma_{pp} + N_1N_2\sigma_{nn} + \zeta\sigma_{np}}{A_1A_2}, \tag{36}$$

$\zeta = Z_1N_2 + N_1Z_2$,

$$\sigma_{np} = \left(-70.67 - 18.18\beta^{-1} + 25.26\beta^{-2} + 113.85\beta\right) \times f_m(np), \tag{37}$$

$$\sigma_{pp} = \sigma_{nn} = \left(13.73 - 15.04\beta^{-1} + 8.76\beta^{-2} + 68.67\beta^4\right) \times f_m(nn), \tag{38}$$

where

$$\beta = \frac{v}{c} = \sqrt{1 - \left(\frac{931.5}{\varepsilon_{lab} + 931.5}\right)^2} \tag{39}$$

is the ratio of the relative to the light velocities, $\epsilon_{lab} = E/A_1$ is the energy (in MeV) of a nucleon in the incident nucleus in the laboratory system [1], and cross sections are given in mb. The factors $f_m(np)$ and $f_m(nn)$ are introduced to correct the dependence of cross sections on the energy and on the density of nuclear matter. The in-medium NN interaction has been widely investigated. For instance, in [73] numerical calculations of the total NN cross sections have been performed on the basis of

[1] In our case one has $Z_1 = A_1 = 1, N_1 = 0$.

the Dirac-Brueckner theory of nuclear matter and their parametrization has been given in ref. [74] to obtain the following correcting factors:

$$f_m(np) = \frac{1 + 20.88\varepsilon_{lab}^{0.04}\rho^{2.02}}{1 + 35.86\rho^{1.90}}, \quad (40)$$

$$f_m(nn) = \frac{1 + 7.772\varepsilon_{lab}^{0.06}\rho^{1.48}}{1 + 18.01\rho^{1.46}}. \quad (41)$$

In eqs. (40) and (41) the densities are in fm^{-3}. In the case of free nucleons (ρ=0) $f_m(np)$=$f_m(nn)$=1. The increase of the density leads to decrease of these factors and, correspondingly, of the cross sections.

Here we present also the ratio of the real to imaginary part of the NN amplitude at zero angle averaged over the nuclear isospins and parametrized in [72]:

$$\bar{\alpha}_{NN} = \frac{Z_1Z_2\alpha_{pp}\sigma_{pp} + N_1N_2\alpha_{nn}\sigma_{nn} + \zeta\alpha_{np}\sigma_{np}}{Z_1Z_2\sigma_{pp} + N_1N_2\sigma_{nn} + \zeta\sigma_{np}}, \quad (42)$$

$$\alpha_{nn} = \alpha_{pp} = 0.0078 + 0.1762\sqrt{\varepsilon_{lab}} + 0.01436\varepsilon_{lab}, \quad (43)$$

$$\alpha_{np} = -0.0301 + 0.2148\sqrt{\varepsilon_{lab}} - 0.0551\varepsilon_{lab}. \quad (44)$$

The results of calculations of the ^{6}He+p elastic scattering cross sections at energy 41.6 MeV/N using the OP in the form (33) are presented in fig. 4 with and without spin-orbita term of the form of $0.5\lambda_\pi^2(\mathrm{d}/\mathrm{d}r)V^{micro}$. It is seen a better agreement with the data up to $\vartheta \simeq 40^\circ$ in the case when the spin-orbit term is included. The LSSM densities of ^{6}He have been used in the calculations. Here we would like to mention the question whether the data can be reasonably fitted either by introducing a spin-orbit force, or by renormalizing the potential. For the folding potential these two ways are not equivalent because of the role of the spin-orbit term at large angles. However, in the case of the HEA, responsible for the area of comparably small angles, it seems likely that one could fit the data using either a spin-orbit term or a renormalization. We note, however, that our main goal is to show that the HEA OP's can be used in their domain of validity with no additional free parameters; this is certainly true with the inclusion of the spin-orbit term at angles smaller than 40°.

In the next sect., following the basic theoretical scheme given in sects. 2 and 3, we present the results of our calculations. For calculations of Re OP we use the effective M3Y interaction based on the Paris NN potential with a density dependence in the form CDM3Y6 from [38] without "regularization". Also we account for the spin-orbit term $\sim\mathrm{d}V^{micro}/\mathrm{d}r$ and use the LSSM proton and neutron densities of ^{6}He. Besides, we include in the calculations the imaginary part of the OP's obtained within the HEA.

4 Results of calculations and discussion

In this sect. we present our calculations of the cross sections of ^{6}He+p elastic scattering at different energies aiming to study: i) effects of the different behavior of the model densities of ^{6}He; ii) the possibility to use the HEA optical potentials for different energies and angles and also the microscopic OP with the folded real part $V^F = V^D + V^{EX}$ and the HEA imaginary part W^H; iii) the role of the renormalization of the depths of the real and imaginary parts of OP's, and iv) the in-medium effects of the effective NN interaction on the microscopically calculated Re OP.

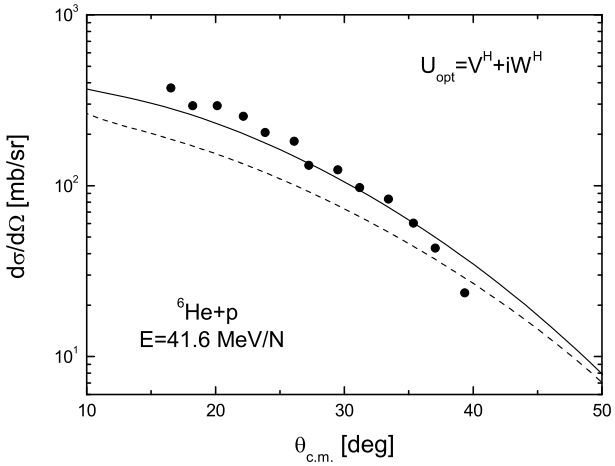

Fig. 4. Elastic ^{6}He+p scattering cross section at energy E = 41.6 MeV/N calculated by using $U_{opt} = V^H + iW^H$ with (solid line) and without (dashed line) spin-orbit term $(1/r)\mathrm{d}V^H/\mathrm{d}r$. The ^{6}He LSSM density is used. Experimental data are from refs. [6,8].

We start this sect. with calculations of the ^{6}He+p elastic cross sections using the real part of OP calculated within the folding approach (V^F), as well as the real (V^H) and imaginary (W^H) parts of the HEA OP's. We introduce two renormalization parameters N_R and N_I (already mentioned above) and consider the following three types for the OP's:

$$(A) \qquad U_{opt}^A = N_R^A V^H + iN_I^A W^H, \quad (45)$$

$$(B) \qquad U_{opt}^B = N_R^B V^F + iN_I^B W^H, \quad (46)$$

$$(C) \qquad U_{opt}^C = N_R^C V^F + iN_I^C V^F. \quad (47)$$

As can be seen, in case (A) we use both real and imaginary parts from the HEA calculations of OP's; in case (B) we take V^F, the folded real part of the microscopic OP where the exchange term is included, and the imaginary part is applied in the form (35) of the HEA OP, while in case (C) we use the microscopically folded real and imaginary parts in the form of V^F, and thus they have the same shape.

In fig. 5 are presented the results of calculations of the ^{6}He+p elastic cross sections (for energy E=41.6 MeV/N) with the fixed value N_I=1 for all three cases (A), (B) and (C). The comparison with the data is performed for two values of N_R for each case, namely 0.53 and 1.00 for case (A), 0.85 and 1.00 for cases (B) and (C). One can see a good agreement with the data using N_R=1.00 for

the cases (A) and (B) and using $N_R = 0.85$ for case (C). It can be concluded that for both cases (A) and (B) the renormalization is not necessary. As in the case shown in fig. 4, we note that the agreement obtained by using the HEA is for angles smaller than 40°.

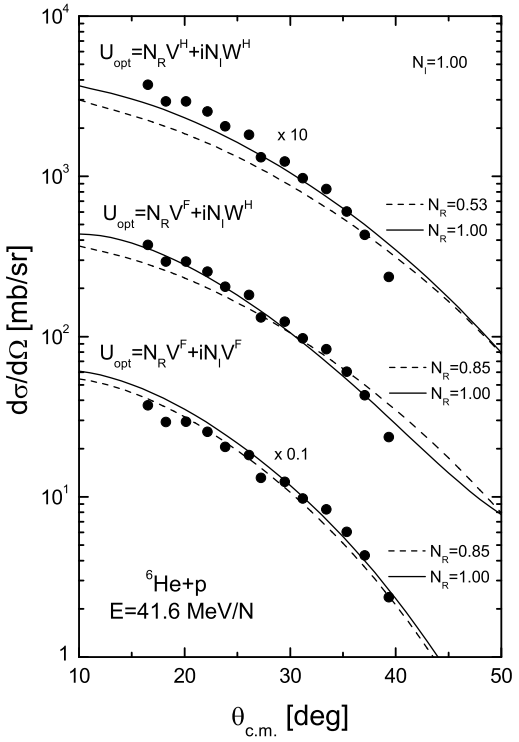

Fig. 5. Elastic ^{6}He+p scattering cross section at energy $E =$ 41.6 MeV/N calculated using different OP's (cases (A), (B) and (C) from the text) for various values of the renormalization parameters N_R ($N_I = 1$). The LSSM density of ^{6}He is applied. Experimental data are from refs. [6,8].

The latter concerns also the results of the calculations of ^{6}He+p elastic scattering (E=41.6 MeV/N) in case (B) using three densities of ^{6}He given by Tanihata *et al.*, COSMA and from the LSSM given in fig. 6. It can be seen a good agreement with the empirical data up to $\vartheta \simeq 35°$. Deviations of the results with the use of the COSMA density from the other two cases start at angles larger than 40°. In these calculations $N_R = N_I = 1$.

In fig. 7 we present the real (V^F) and imaginary (W^H) parts of the OP's (case (B)) calculated using the LSSM density of ^{6}He for three different energies: 25.2, 41.6, and 71 MeV/N. They are given without renormalization (*i.e.* N_R=N_I=1) and are illustrated in logarithmic and linear scales. One can see the decrease of the potential depths with the increase of the energy. Here we would like to note that, as can be seen from fig. 7, at $\bar{R} \approx 2$ fm the values of the potentials for $E_{lab} = 40$ MeV/N are $U(\bar{R}) \approx 15 - 20$ MeV, and thus the limit condition for the HEA $E > U(\bar{R})$ is fulfilled. This explains the applicability of the HEA at such values of the energy. We should mention the larger depth of the HEA imaginary parts (W^H) of the OP for the case of 25.2 MeV/N seen in fig. 7. As we will see below, the result of the HEA for W^H in this case affects significantly the cross section.

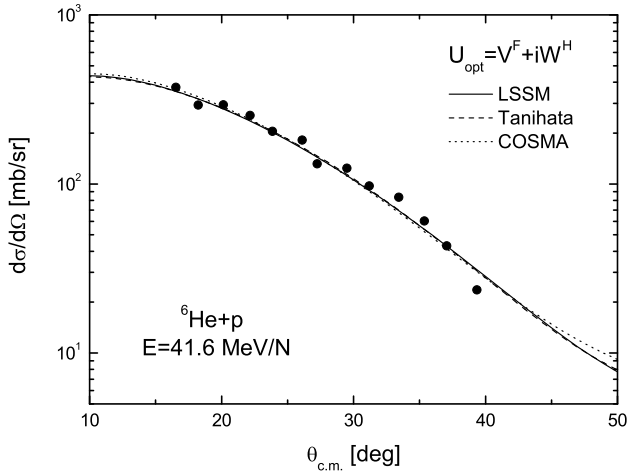

Fig. 6. Elastic ^{6}He+p scattering cross section at energy $E =$ 41.6 MeV/N calculated using $U_{opt} = V^F + iW^H$ and Tanihata (dashed line), COSMA (dotted line) and LSSM (solid line) densities of ^{6}He. Experimental data are from [6,8].

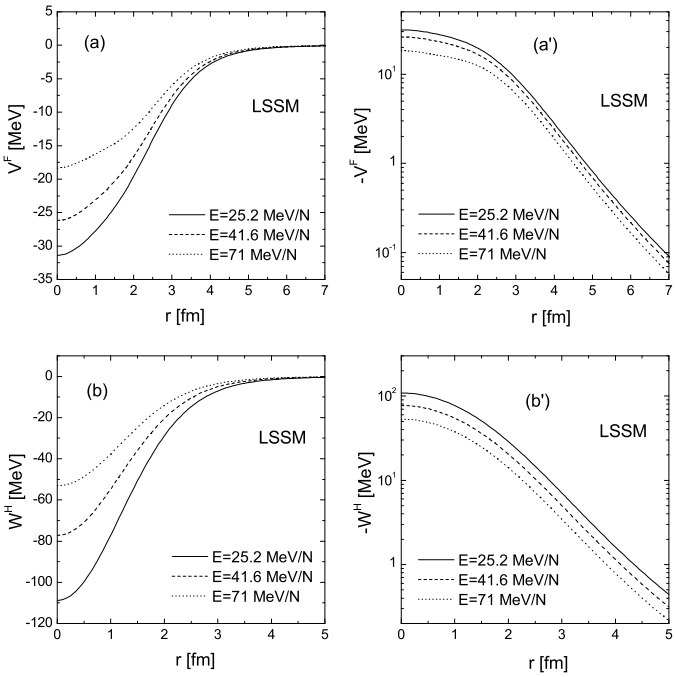

Fig. 7. Microscopic real part (V^F) of OP ((a) and (a′)) and HEA imaginary part (W^H) ((b) and (b′)) calculated using the LSSM density of ^{6}He for energies $E = 25.2$ (solid lines), 41.6 (dashed lines) and 71 MeV/N (dotted lines).

The three densities are used to calculate the cross sections of ^{6}He+p elastic cross sections for three energies (25.2, 41.6, and 71 MeV/N) shown in fig. 8. One can see the fairly good agreement with the experimental data of the results with the LSSM density for ^{6}He for energies

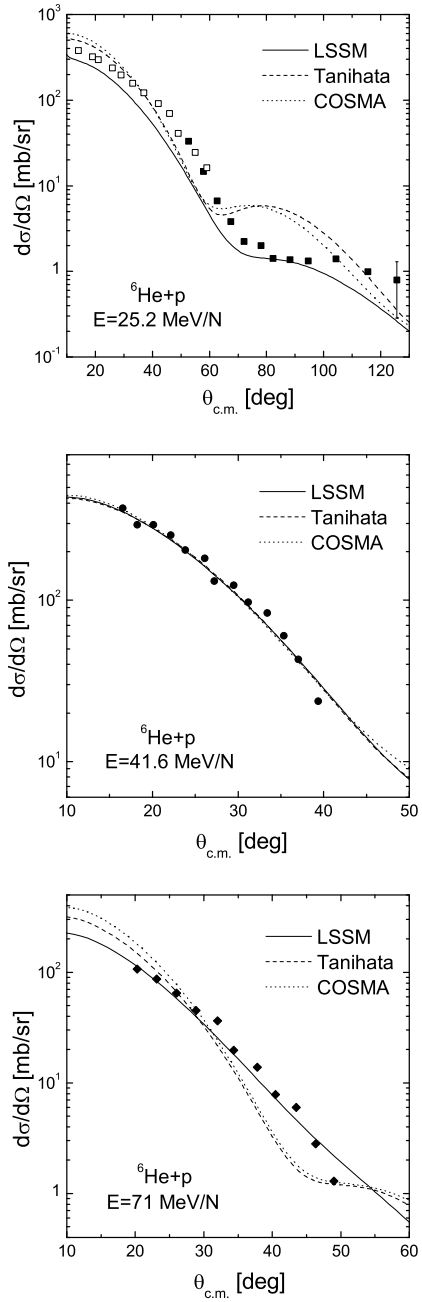

Fig. 8. Elastic ^{6}He+p scattering cross sections at different energies calculated using $U_{opt} = N_R V^F + iN_I W^H$ for various values of the renormalization parameters N_R and N_I giving a reasonable agreement with the data (presented in table 1). The used densities of ^{6}He are LSSM (solid line), Tanihata (dashed line) and COSMA (dotted line). Experimental data are taken for 25.2 [1,2,3], 41.6 [6,8] and 71 MeV/N [9,10].

41.6 and 71 MeV/N, in contrast to the results obtained with the other two densities for the energies 25.2 and 71 MeV/N. In table 1 we list the values of the renormalization parameters N_R and N_I that give a reasonable agreement with the data for the three energies and the three different densities of ^{6}He shown in fig. 8. One can see also the corresponding depths $N_R V_F^{(r=0)}$ and $N_I W_H^{(r=0)}$ of the real and imaginary parts of OP's. The values of N_R and N_I were chosen starting from the values $N_R = 1$ and $N_I = 1$ and decreasing them gradually in order to achieve a reasonable fit to the experimental data. In our opinion, the obtained values of N_R and N_I still do not reveal some regular change with the increase of the energy.

In fig. 9 a particular attention is paid to the case of the elastic ^{6}He+p cross section at energy of 25.2 MeV/N calculated using the LSSM density for the ^{6}He nucleus. One can see that, in contrast to the case of larger energies, in this case smaller values of N_R (0.35) and especially of N_I (0.03) are necessary for a better agreement with the experimental data. This concerns the slope of the cross section for angles $\vartheta_{c.m.}$ between 70° and 120°. We note that the results shown in fig. 9 for the energy 25.2 MeV/N are for angles up to $\vartheta_{c.m.} \approx 120°$. The necessity to use much smaller value of the renormalization parameter N_I ($N_I = 0.03$) to fit the data for large angles is related to the large value of the depth of the imaginary part of the OP obtained within the HEA (W^H) for this case, as already mentioned above. This already shows the limitation of the approach (the case (B), Eq. (46)) for small energies (< 25 MeV/N) and large angle values. In this case the condition $E > |U(\bar{R})|$ is not already fulfilled. Along this line we should mention the Ref. [75] in which a microscopical pseudo-folding potential (without accounting for the exchange) $V_{micro} = (N_R + iN_I)V_{folding}$ was used for calculations of p+^{18}Ne and p+^{18}O scattering at energies 24.5 and 30 MeV/N. It was shown a good agreement with the data with $N_I = 0$ for ^{18}Ne and $N_I = 0.006$ for ^{18}O. These results confirm the necessity to use microscopical rather than phenomenological OP's also for low energy scattering.

In fig. 10 we present the in-medium effect of the NN interaction on the elastic scattering cross sections of ^{6}He+p. The calculations were performed using the function $F(\rho)$ in the form (5) and with $F(\rho)$=1 (the case without in-medium effect). The effective M3Y interaction based on the Paris NN potential and the LSSM density of ^{6}He were used in the calculations. One can see the existence of small differences between the results using density dependent and independent effective NN interaction. The differences for the larger angles increase with the energy increase.

Also, we studied the non-linear effects in calculations of the exchange part of OP. As can be seen, the factor $j_0(k(r) \cdot s)$ takes place in the expressions for the V^{EX} (see eqs. (11), (15) and (19)), where the local momentum of the relative motion $k(r)$ [eq. (20)] is expressed by the OP. The calculations need an iteration procedure and this makes the task complicated. However, if $k(r) \simeq 0$, then $j_0 \simeq 1$ and this simplifies calculations. In fig. 11 we present the results for the ^{6}He+p elastic scattering cross section at different energies with and without accounting for the factor $j_0(k(r) \cdot s)$ in the above mentioned equations. As can be seen, the non-linearity effect is small for the energy $E = 25.2$ MeV/N, but it increases with the energy increase up to an order of magnitude for $\vartheta > 40°$ for the energy $E =$

Table 1. The optimal values of the renormalization parameters N_R and N_I obtained by fitting the experimental data for the elastic ^{6}He+p cross sections. In the calculations $U_{opt} = N_R V^F + iN_I W^H$ and LSSM, Tanihata and COSMA densities for energies E=25.2, 41.6, and 71 MeV/N are used (the results are shown in fig. 8). The depths of the corresponding potentials (in MeV) are presented, as well.

Energy	25.2	25.2	41.6	41.6	71	71
Density	N_R	N_I	N_R	N_I	N_R	N_I
LSSM	0.6	0.8	1.0	1.0	0.6	1.0
Tanihata	1.0	0.6	1.0	1.0	1.0	0.5
COSMA	1.0	0.6	1.0	1.0	0.8	1.0
Energy	25.2	25.2	41.6	41.6	71	71
Density	$N_R V_F^{(r=0)}$	$N_I W_H^{(r=0)}$	$N_R V_F^{(r=0)}$	$N_I W_H^{(r=0)}$	$N_R V_F^{(r=0)}$	$N_I W_H^{(r=0)}$
LSSM	18.86	87.02	26.22	77.20	11.01	53.09
Tanihata	30.82	39.15	25.54	46.31	17.56	15.92
COSMA	29.70	30.05	24.73	35.54	13.78	24.44

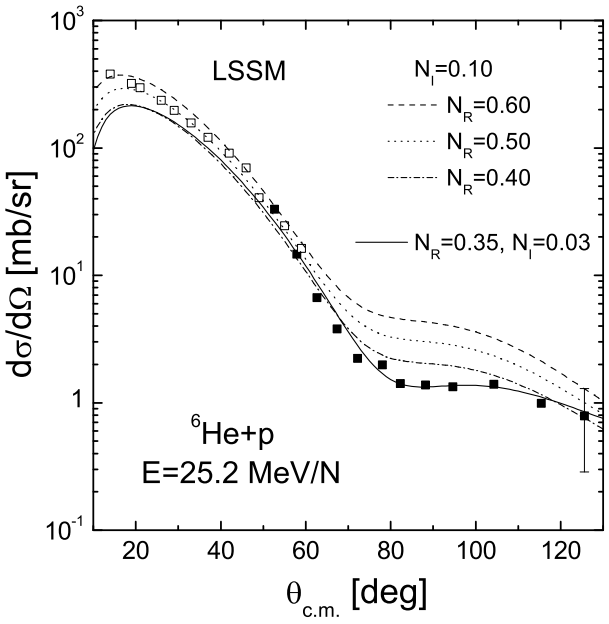

Fig. 9. Elastic ^{6}He+p scattering cross sections for E = 25.2 MeV/N calculated by using the LSSM density for ^{6}He. The curves exhibit results for $U_{opt} = N_R V^F + iN_I W^H$ with different values of N_R (0.6-dashed, 0.5-dotted, 0.4-dash-dotted) and fixed value of N_I=0.1. The solid curve is for N_R=0.35 and N_I=0.03. The experimental data [1,2,3] are also given.

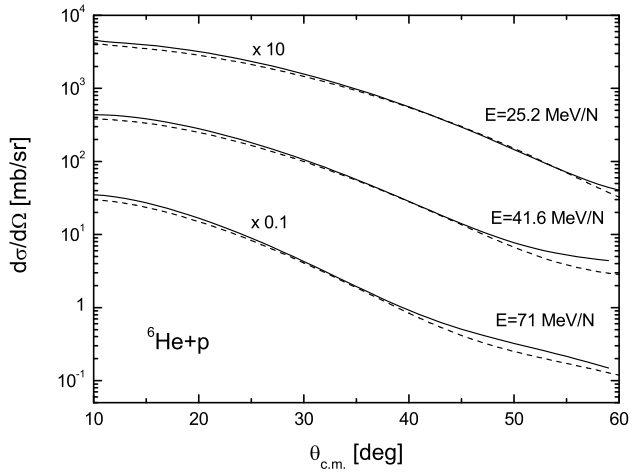

Fig. 10. In-medium effect of the M3Y NN interaction on calculations of elastic ^{6}He+p scattering cross sections for different energies. The Re OP (V^F) is calculated with $F(\rho) = C(1+\alpha\exp(-\beta\rho)-\gamma\rho)$ (solid lines) and with $F(\rho) = 1$ (dashed lines). The imaginary part is calculated within the HEA (W^H).

71 MeV/N. These results show the necessity to perform calculations accounting for the non-linearity of the task.

5 Conclusions

The results of the present work can be summarized as follows:

i) The optical potentials and cross sections of ^{6}He+p elastic scattering were calculated at three different energies E = 25.2, 41.6, and 71 MeV/N. The following components of the OP's were used:

a) the real part of the OP (V^F) calculated microscopically using the folding procedure and M3Y effective interaction based on the Paris NN potential;

b) the real (V^H) and imaginary (W^H) parts of the OP calculated within the high-energy approximation (HEA);

c) three different combinations of V^F, V^H and W^H (cases (A), (B) and (C), eqs. (45)-(47)) were used for the OP U_{opt} in calculations of the elastic ^{6}He+p cross sections. The renormalization parameters N_R and N_I have been introduced and their role has been studied.The cross sections were calculated by numerical integration of the Schrödinger equation by means of DWUCK4 code using

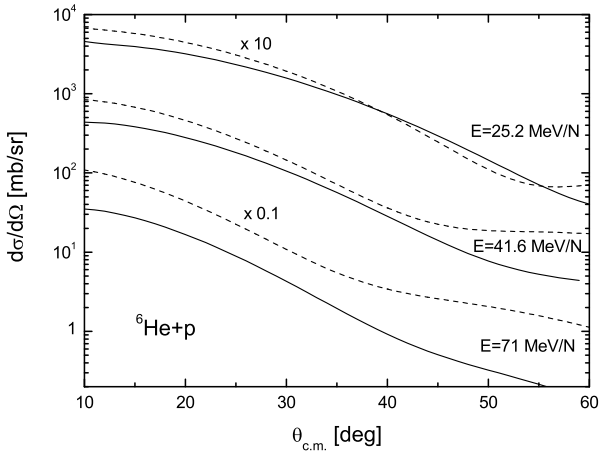

Fig. 11. The non-linearity effect of elastic ^{6}He+p scattering cross section for different energies. The solid lines are the calculation results when Re OP (V^F) includes $j_0(k(r)\cdot s)$ term in eq. (11) and the dashed lines are without this term. The LSSM density of ^{6}He is used. The imaginary part of OP is calculated within the HEA (W^H).

all interactions obtained (Coulomb plus nuclear optical potential);

d) three different model densities of protons and neutrons in ^{6}He were used in the calculations: the phenomenological ones in the form (30), parametrized by Tanihata *et al.*, the same form (30) with parameters from the COSMA, and also the microscopically calculated density within the LSSM.

ii) The results of our calculations show that the LSSM density of ^{6}He is the most preferable one because it leads to a better agreement with the data for the ^{6}He+p elastic scattering at the three energies. The physical reason for the latter is that the LSSM densities have more diffuse tails at larger r than the densities based on Gaussians. With the LSSM density and with the optical potentials of the form (B), namely $U_{opt} = N_R V^F + iN_I W^H$, we tried to choose the parameters N_R and N_I starting from the values $N_R = 1$ and $N_I = 1$ and decreasing them gradually in order to achieve a reasonable agreement of the calculated cross sections with the available data. The obtained set of these parameters is the following one: $N_R = 0.6$, 1.0 and 0.6 and $N_I = 0.8$, 1.0 and 1.0 for energies 25.2, 41.6, and 71 MeV/N, respectively. We note that the use of the microscopic folding real part V^F and of the HEA imaginary part W^H leads to a good agreement with the data for 41.6 and 71 MeV/N, while the data at lowest energy 25.2 MeV/N are explained only on the qualitative level. As shown by the estimations presented, this is related to the limitations of using the imaginary part of the HEA OP for energy smaller than around 25 MeV/N due to the fact that the potentials do not fulfill the applicability condition $E > |U(\bar{R})|$. In this case the large value of the depth of the Im OP obtained in the HEA W^H has to be strongly reduced (*e.g.* using in our case $N_I = 0.03$) in order to achieve a reasonable agreement with the data for the energy 25.2 MeV/N.

iii) It was shown that the effect of the regularization of the M3Y NN effective interaction is rather weak (with a small increase with the increase of the energy and the angle) and, our conclusion is that it is not necessary to use it applying the folding approach to the cases of nucleon-nucleus scattering.

iv) The results show that the spin-orbit interaction is rather important, particularly at angles larger than 60°, and that one can use in the ls-term the microscopically calculated Re OP instead of the phenomenological WS potential with the three fitted parameters.

v) The study of the dependence of the effective M3Y NN forces on the nuclear matter density shows small differences between optical potentials calculated with and without inclusion of the in-medium effect. The difference between the corresponding cross sections appears at larger angles and increases with the energy increase.

vi) We showed that the effect of the non-linearity on calculations of Re OP connected with the factor $j_0(k(r)\cdot s)$, where $k(r)$ is the local momentum of motion, is small for the energy of 25.2 MeV/N but it increases with the energy increase up to an order of magnitude for $\vartheta_{c.m.} > 40°$ for the energy $E = 71$ MeV/N. Thus, the non-linearity in the calculations of the Re OP should be taken into account in the calculations.

Concluding, we would like to note that it follows from our results that the OP's can be calculated in the form $U^B_{opt} = N_R V^F + iN_I W^H$ (*i.e.* with microscopically calculated folding real part (V^F) and with calculated within HEA imaginary part (W^H)) using only two free parameters (N_R and N_I) which renormalize the depths of the real and imaginary parts of OP. Thus, it is not necessary (at least on the basis of the existing experimental data on ^{6}He+p elastic scattering cross sections) to introduce a large number of fitting parameters, as is usually done in the arbitrarily chosen forms of the phenomenological and semi-microscopic optical potentials. It was pointed out that our approach can be applied to cases with energies smaller than 100 MeV/N, like those of 71 MeV/N and 41.6 MeV/N considered in the present work. It can be concluded that microscopical optical potentials (including their imaginary part, *e.g.* of the HEA-type) rather than phenomenological ones have to be applied also for the cases of tens of MeV/N. Thus the approach can be used along with other more sophisticated methods like that from the microscopic g-matrix description of the complex proton optical potential and others.

The work is partly supported on the basis of the Project from the Agreement for co-operation between the INRNE (Sofia) and JINR (Dubna). Two of the authors (A.N.A. and M.K.G.) are grateful for the support of the Bulgarian Science Fund under Contracts Nos. Φ–1416 and Φ–1501. The author M.K.G. is grateful for the warm hospitality given by the CSIC and for support during his stay there from the State Secretariat of Education and Universities of Spain (N/Ref. SAB2005–0012). The authors E.V.Z. and K.V.L. thank the Russian Foundation for Basic Research (Grant No. 06-01-00228) for the partial support.

References

1. G.M. Ter-Akopian *et al.*, Phys. Lett. B **426**, 251 (1999); G.M. Ter-Akopian *et al.*, in *Fundamental Issues in Elementary, Proceedings of the Symposium in honor and memory of Michael Anos, Bad Honnef, Germany, 2000*, edited by W. Greiner (E P Systema, Debrecen, 2001), p.371.
2. R. Wolski *et al.*, JINR Preprint E15-98-284, 1998; Phys. Lett. B **467**, 8 (1999); S. Stepantsov *et al.*, Phys. Lett. B **542**, 35 (2002).
3. L. Giot *et al.*, Nucl. Phys. A **738**, 426 (2004).
4. K. Rusek, K.W. Kemper, R. Wolski, Phys. Rev. C **64**, 044602 (2001).
5. V. Lapoux *et al.*, Phys. Lett. B **517**, 18 (2001).
6. M.D. Cortina-Gil *et al.*, Nucl. Phys. A **616**, 215c (1997).
7. A. Lagoyannis *et al.*, Phys. Lett. B **518**, 27 (2001).
8. M.D. Cortina-Gil *et al.*, Phys. Lett. B **371**, 14 (1996).
9. A.A. Korsheninnikov *et al.*, Nucl. Phys. A **616**, 189c (1997).
10. A.A. Korsheninnikov *et al.*, Nucl. Phys. A **617**, 45 (1997).
11. G.D. Alkhazov *et al.*, Nucl. Phys. A **712**, 269 (2002).
12. P. Egelhof, Prog. Part. Nucl. Phys. **46**, 307 (2001).
13. P. Egelhof, Eur. Phys. J. A **15**, 27 (2002).
14. S.R. Neumaier *et al.*, Nucl. Phys. A **712**, 247 (2002).
15. P. Egelhof, O. Kisselev, G. Münzenberg, S.R. Neumaier, H. Weick, Phys. Scr. **104**, 151 (2003) (and references therein).
16. L.L. Chulkov, C.A. Bertulani, A.A. Korsheninnikov, Nucl. Phys. A **587**, 291 (1995).
17. R. Crespo, J.A. Tostevin, R.C. Johnson, Phys. Rev. C **51**, 3283 (1995).
18. M.V. Zhukov, B.V. Danilin, D.V. Fedorov, J.M. Bang, I.J. Thompson, J.S. Vaagen, Phys. Rep. **231**, 151 (1993).
19. M.V. Zhukov, A.A. Korsheninnikov, M.H. Smedberg, Phys. Rev. C **50**, R1 (1994).
20. M. Avrigeanu, G.S. Anagnostatos, A.N. Antonov, J. Giapitzakis, Phys. Rev. C **62**, 017001 (2000).
21. M. Avrigeanu, G.S. Anagnastatos, A.N. Antonov, V. Avrigeanu, Int. J. Mod. Phys. E **11**, 249 (2002).
22. P.J. Dortmans, K. Amos, S. Karataglidis, J. Raynal, Phys. Rev. C **58**, 2249 (1998).
23. S. Karataglidis, B.A. Brown, K. Amos, P.J. Dortmans, Phys. Rev. C **55**, 2826 (1997).
24. K. Amos, W.A. Richter, S. Karataglidis, B.A. Brown, Phys. Rev. Lett. **96**, 032503 (2006).
25. P.K. Deb, B.C. Clark, S. Hama, K. Amos, S. Karataglidis, E.D. Cooper, Phys. Rev. C **72**, 014608 (2005).
26. P.K. Deb, K. Amos, S. Karataglidis, M.B. Chadwick, D.G. Madland, Phys. Rev. Lett. **86**, 3248 (2001).
27. P.K. Deb, K. Amos, Phys. Rev. C **67**, 067602 (2003).
28. K. Amos, P.J. Dortmans, H.V. von Geramb, J. Raynal, Adv. Nucl. Phys. **25**, 275 (2000).
29. H.F. Arellano, M. Girod, arXiv: 0706.2693 [nucl-th].
30. R.J. Glauber, *Lectures in Theoretical Physics*, (Interscience, New York, 1959), p.315.
31. A.G. Sitenko, Ukr. Fiz. Zh., **4**, 152 (1959).
32. R.F. Casten, B.M. Sherrill, Prog. Part. Nucl. Phys. **45**, S171 (2000).
33. G.D. Alkhazov *et al.*, Phys. Rev. Lett. **78**, 2313 (1997).
34. R.J. Satchler, W.G. Love, Phys. Rep. **55**, 183 (1983); R.J. Satchler, *Direct Nuclear Reactions*, (Clarendon, Oxford, 1983).
35. D.T. Khoa, W. von Oertzen, Phys. Lett. B **304**, 8 (1993); **342**, 6 (1995); D.T. Khoa, W. von Oertzen, H.G. Bohlen, Phys. Rev. C **49**, 1652 (1994); D.T. Khoa, W. von Oertzen, A.A. Ogloblin, Nucl. Phys. A **602**, 98 (1996); D.T. Khoa, H.S. Than, nucl-th/0502059.
36. S. Karataglidis, P.J. Dortmans, K. Amos, C. Bennhold, Phys. Rev. C **61**, 024319 (2000).
37. K. Amos, *Proceedings of the 9th Conference on Nuclear Reaction Mechanisms, Varenna, 2000*, edited by E. Gadioli (Ricerca Scientifica, Milano, 2000), p.51.
38. D.T. Khoa, G.R. Satchler, Nucl. Phys. A **668**, 3 (2000).
39. N. Anantaraman, H. Toki, G. Bertsch. Nucl. Phys. A **398**, 279 (1983).
40. I. Tanihata, Phys. Lett. B **289**, 261 (1992) (and references therein).
41. K.V. Lukyanov, E.V. Zemlyanaya, V.K. Lukyanov, JINR Preprint P4-2004-115, 2004; Phys. At. Nucl. **69**, 240 (2006).
42. K.M. De Vries, J.C. Peng, Phys. Rev. C **22**, 1055 (1980).
43. A. Vitturi, F. Zardi, Phys. Rev. C **36**, 1404 (1987).
44. S.K. Charagi, S.K. Gupta, Phys. Rev. C **41**, 1610 (1990); Phys. Rev. C **46**, 1982 (1992).
45. S.K. Charagi, S.K. Gupta, Phys. Rev. C **56**, 1171 (1997).
46. R. Liguori Neto *et al.*, Nucl. Phys. A **560**, 733 (1993).
47. D.M. Brink, G.R. Satchler, J. Phys. G **7**, 43 (1981).
48. P. Shukla, Phys. Rev. C **67**, 054607 (2003).
49. X. Campy, A. Bouyssy, Phys. Lett. B **73**, 263 (1978).
50. J.W. Negele, D. Vautherin, Phys. Rev. C **5**, 1472 (1972).
51. D.T. Khoa, E. Khan, G. Coló, N. Van Giai, Nucl. Phys. A **706**, 61 (2002).
52. P. Ring, P. Schuck, *The Nuclear Many-Body Problem*, (Springer-Verlag, New-York, 1980), p.542.
53. D.T. Khoa, Phys. Rev. C **63**, 034007 (2001).
54. M. Avrigeanu, A.N. Antonov, H. Lenske, I. Stetcu, Nucl. Phys. A **693**, 616 (2001).
55. R. Machleidt, Adv. Nucl. Phys. **19**, 189 (1989).
56. V.G.J. Stoks, R.A.M. Klomp, C.P.F. Terheggen, J.J. de Swart, Phys. Rev. C **49**, 2950 (1994).
57. V.R. Pandharipande, *Correlations and Clustering Phenomena in Subatomic Physics*, edited by M.N. Harakeh, J.H. Koch and O. Scholten (Plenum Press, New York, 1997), p.1.
58. V.G. Stoks, R. Timmermans, J.J. de Swart, Phys. Rev. C **47**, 512 (1993).
59. H. Chandra, G. Sauer, Phys. Rev. C **13**, 245 (1976).
60. I. Tanihata *et al.*, Phys. Rev. Lett. **55**, 2676 (1985).
61. P.J. Karol, Phys. Rev. C **11**, 1203 (1975).
62. F.D. Becchetti Jr., G.W. Greenlees, Phys.Rev. **182**, 1190 (1969).
63. J.H. Sørensen, A. Winther, Nucl.Phys. A **550**, 329 (1992).
64. D. Gupta, E. Khan, Y. Blumenfeld, nucl-th/0601073.
65. V.K. Lukyanov, E.V. Zemlyanaya, Int. J. Mod. Phys. E **10**, 169 (2001).
66. E.V. Zemlyanaya *et al.*, Izv. Akad. Nauk, Ser. Fiz., **69**, 1649 (2005).
67. E.V. Zemlyanaya *et al.*, *Nuclear Theory, Proceedings of the 25th Int. Workshop on Nucl. Theory, Rila Mountains, Bulgaria, 2006*, edited by S.S. Dimitrova, (Diomira, Sofia, 2006), p.301.
68. P. Roussel-Chomaz *et al.*, Nucl. Phys. A **477**, 345 (1988).
69. W. Czyż, L.C. Maximon, Ann. Phys. **52**, 59 (1969).
70. J. Formanek, Nucl. Phys. B **12**, 441 (1969).

71. G.D. Alkhazov, S.L. Belostotsky, A.A. Vorobyov, Phys. Rep. C **42**, 89 (1978).
72. P. Shukla, nucl-th/0112039.
73. G.Q. Li, R. Machleidt, Phys. Rev. C **48**, 1702 (1993); **49**, 566 (1994).
74. C. Xiangzhou, F. Jun, S. Wenqing, M. Yugang, W. Jiansong, Y. Wei, Phys. Rev. C **58**, 572 (1998).
75. D. Gupta, D.N. Basu, Nucl. Phys. A **748**, 402 (2005).